Journal of
Ceramic Science
and Technology

J. Ceram. Sci. Technol., **16** [3] 107-116 (2025)
DOI: 10.4416/JCST2024-00014
available online at: http://www.ceramic-science.com

Thermomechanical and Thermochemical Behaviour of Silica- and Spinel-Sol-Bonded High-Alumina Refractory Castables

E. Brochen*[1], C. Dannert[1], M. Thiesen[2], T. Ibarra[2], O. Krause[2], S. Abdelouhab[3], C. Lang[3]

[1]Forschungsgemeinschaft Feuerfest e. V. at the European Centre for Refractories, Höhr-Grenzhausen, Germany
[2]Koblenz University of Applied Sciences, WesterWaldCampus, Germany
[3]BCRC-INISMa, Belgian Ceramic Research Centre, Mons, Belgium

received August 8, 2024; received in revised form June 18, 2025; accepted June 22, 2025

Abstract

While calcium aluminate cements have become established as a "workhorse" for refractory castables (reliable and cost-effective), they nonetheless have certain drawbacks (high risk of explosive spalling during drying, limited resistance to acidic slags and ashes) and, after years of optimization, only limited potential remains for further improvements. By contrast, colloidal suspensions (sols) are increasingly used as bonding solutions in the industry (silica sols) and, despite their current limitations (providing low green strength and limited refractoriness), they have much to offer. Especially alternative sols, such as mullite and spinel sols, are attracting attention for improving the refractoriness and resistance to corrosion of sol-bonded castables, but studies regarding their performance at high temperature are extremely sparse.

The thermomechanical and thermochemical behaviour of silica- and spinel-sol-bonded high-alumina refractory castables was investigated using wedge splitting measurements, high-temperature thermal shocks and induction furnace tests. Silica-sol-bonded high-alumina refractory castables are rather weak when compared to high-alumina refractory bricks, but they are able to develop more ductility before weakening and exhibit improved resistance to high-temperature thermal shocks. The use of spinel sols considerably improved the high-temperature mechanical and fracture resistance of the sol-bonded high-alumina refractory castables without degrading their resistance to thermal shocks. The spinel sols even slightly improved the resistance of the castables to corrosion.

Keywords: Refractory castables, colloidal-bonded, high-temperature thermal shocks, wedge splitting test, corrosion resistance.

I. Introduction

Refractory producers are constantly requested to develop refractory solutions that deliver longer lifetimes under increasingly demanding and dynamic application conditions. Historically, refractory linings were typically built with bricks. Over the past few decades, mainly because they simplify and speed up the installation process, monolithic linings have gained in popularity, and become increasingly adopted by refractory user industries. For refractory castables (used to make monolithic linings), the bonding phases (binders) are a key component. Without binders, no monolithics can be produced regardless of whether the product is prepared on site or shaped in the workshops of refractory producers. Improving existing binders or developing new binder solutions that perform better in service and show efficient placing (that is: during installation and before the first heat-up) properties is of high value for user industries that rely on refractory products.

* Corresponding author: brochen@fg-feuerfest.de

Furthermore, the bonding phases of refractory castables play a central role in their performance. Especially their behaviour at high temperature is crucially responsible for the performance of a refractory lining. However, all conventional binder solutions have their weaknesses: 1) The use of the well-established calcium aluminate cement (CAC) as binder reduces the refractoriness in thermochemically aggressive environments, as the calcium contained in the cement reacts with slags, fly ashes or gases to form low-melting-point compounds and can lead to premature deterioration of the linings. 2) Hydratable alumina (HA) binder leads to better performance at high temperature for refractory castables exposed to thermochemically aggressive environments. However, the drying and first heating of HA-bonded refractory castables has to be performed with the greatest care to avoid explosive spalling induced by the massive release of chemically bonded water and the corresponding huge steam pressure. 3) CS (colloidal silica)-bonded refractory castables like those currently available on the market perform better than CAC- or HA-bonded refractory castables with

regard to their drying behaviour and their inertness when exposed to fly ashes or process gases [1]. This is because a colloidal solution (= sol) is used to bond the refractory castables after gelling (= formation of a gel) with a minimal amount of chemically bonded water that can be easily removed during the drying process and first heat-up. However, their high-temperature performance is limited due to the presence of free amorphous silica, leading to the formation of viscous/liquid phases at high temperature [1–2] and thereby reducing their thermomechanical resistance. In this regard, alternative colloidal suspensions (sols), such as mullite or spinel sols, are currently being considered as binders for refractory castables. That being said, the aspects of characterization and accordingly understanding the high-temperature behaviour of colloidal-bonded castables remains under-documented. Mainly results from relatively straightforward characterization methods can be found in the literature, namely the hot modulus of rupture (HMOR) [3–9], standard thermal shock measurements (i.e. below 1 200 °C) [4–11] and a standard test method for isothermal corrosion resistance (cup test) [9–13]. These are, however, not qualified to accurately depict the high-temperature thermomechanical and thermochemical behaviour of colloidal-bonded monolithic linings. Beyond that, solely material characterization (bulk density, open porosity, cold crushing strength and modulus of rupture on pre-fired test pieces) at room temperature has been reported. Such investigations only provide limited information about the behaviour of refractory castables in service conditions.

II. Testing Strategy

The key to understanding and predicting the behaviour of refractory products during service lies to a great extent in the capacity to reproduce and actively monitor the behaviour of the material in the laboratory. With focus on an industrial application for the prominent steelmaking industry, two main investigation paths were therefore followed to ensure a comprehensive study of the behaviour of model colloidal-bonded high-alumina refractory castables. Firstly, thermomechanical investigations were performed, focusing on assessment of the fracture behaviour based on wedge splitting measurements, as well as the characterization of the resistance to thermal shocks under practice-relevant conditions. In parallel, thermochemical investigations, specifically the assessment of the resistance to corrosion, were conducted using induction furnace tests to simulate the corrosion process in a steel ladle.

III. Materials and Methods

(1) Colloidal-bonded high-alumina refractory castables

Two different base formulations were developed, a fine variant (F) and a coarse variant (C). Both variants are model high-alumina spinel-containing castables with a well-defined grain size distribution (Table 1). The main aggregates are tabular alumina T60/T64 (Almatis, Ludwigshafen, Germany), a sintered α-alumina material (Al_2O_3 > 99 wt%) that has been fully densified by means of rapid sintering at temperatures in excess of 1 800 °C, Spinel AR 78 (Almatis, Ludwigshafen, Germany), a synthetic alumina-rich spinel and E-SY2000 (Almatis, Ludwigshafen, Germany), a high-chemical-purity bi-modal reactive alumina containing besides

Table 1: Composition of the model colloidal-bonded high-alumina refractory castables in wt%.

Castable	F-Ref	C-Ref	CSPS30	CSPS50
Tabular alumina (T60/T64)				
3,0 – 6,0 mm	5	23	23	23
1,0 – 3,0 mm	10	20	20	20
0,5 – 1,0 mm	10	10	10	10
0,2 – 0,6 mm	5			
0,0 – 0,5 mm	18	15	15	15
0,0 – 0,2 mm	20			
0 – 0,045 mm	10			
AR 78		10	10	10
E-SY2000	20	20	20	20
Silica Sol – Lithosol 1530 (30 % solid content)	**5**	**5**	-	-
Spinel Sol (30 % solid content)	-	-	**5**	-
Spinel Sol (50 % solid content)	-	-	-	**5**
Dispersing agent (Castament FS20)	0,1	0,1	0,1	0,1
Additional water	2,5	1,5	1,5	1,5

alumina a defined amount of ultrafine alumina-rich spinel (~ 50 wt%). The fine variant (F-Ref) was specifically designed to be more reactive in order to promote an early formation of mullite while using the commercial silica sol (Lithosol 1530 from Zschimmer & Schwarz Holding GmbH & Co KG, Lahnstein, Germany). The coarse variant was developed to be both closer to the castable formulations commonly used by end-user industries and relatively simple in its composition in order to investigate the potential benefits of using alternative colloidal suspensions, specifically those based on spinel instead of silica. The preparation methods for these suspensions are detailed elsewhere [14]. For a concise comparison of the properties of the colloidal suspensions used, please refer to Table 2.

Table 2: Zeta potential and particle size analysis.

Colloidal suspension	Zeta potential (mV)	D15 (nm)	D50 (nm)	D85 (nm)
Silica Sol – Lithosol 1530 (30 % solid content)	-39,7	12	17	22
Spinel Sol (30 wt%)	-54.5	47	74	116
Spinel Sol (50 wt%)	-45.2	52	80	123

For comparative purposes, a commercially available formulation (IN) from the company Refratechnik Steel was additionally investigated.

After mixing in an intensive mixer (type R05, Maschinenfabrik Gustav Eirich) for the fine variant (F) or a stand mixer (KitchenAid 5KSM7990XESL 325 W) for the coarser variant (C), the model castables were cast into custom-made moulds to produce ∅ 50 × 102 mm cylinders for the thermal shock resistance investigations, 100 × 100 × 75 mm prisms for the investigations of the fracture behaviour and trapezoidal prisms for the corrosion investigations.

All cast pieces were stored for 24 h to cure in open air conditions. Then they were demoulded to be dried at 100 °C for 24 h and finally pre-fired at 800 °C for 5 hours to stabilize the microstructure at the temperature used in the standby furnace before the thermal shocks were applied. ∅ 50 × 102 mm cylinders were cut in half to obtain test pieces measuring ∅ 50 × 50 mm.

(2) Thermomechanical characterization

(a) *Wedge splitting measurements*

Being able to promote the stable fracture of large test pieces, the Wedge Splitting Test (WST) has become established for investigation of the fracture behaviour of coarse-grain materials such as concretes and refractory materials [15]. The test piece geometry and details of the test principle are shown in the Fig. 1. A cubic test piece (100 × 100 × 75 mm) is prepared including a starter notch and two guide notches. Moreover, a large groove is machined into the test piece to accommodate the mechanism that transmits the load applied on a wedge into the test piece.

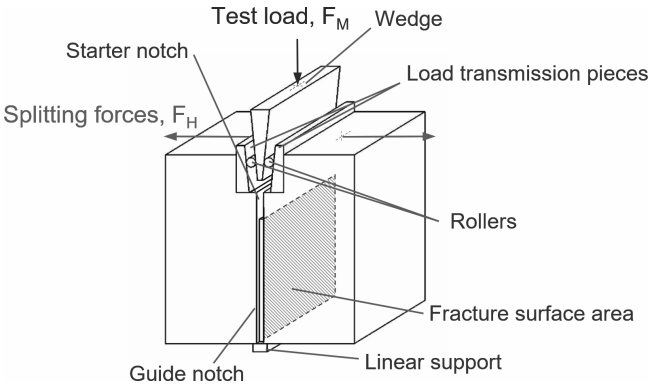

Fig. 1: Principle of the wedge splitting test.

During a test, the vertical force F_M applied by a press is converted into two horizontal forces F_H by means of a prismatic wedge and the load transmission pieces. The two horizontal forces then cause the test piece to split, promoting a stable propagation of cracks despite a high fracture area (approx. 65 mm × 65 mm). During the whole fracture process, the applied load and the opening of the test piece δ_H are recorded and plotted in a load-displacement diagram.

The specific fracture energy G_f is calculated by integrating the horizontal force on the opening of the test piece, usually called horizontal displacement δ_H:

$$G_F = \frac{1}{A}\int_0^{\delta_{ult}} F_H \, d\delta_H \tag{1}$$

δ_{ult} corresponds to the ultimate horizontal displacement (opening) of the test piece during the wedge splitting measurement and A is the fracture surface area. In addition, a nominal notch tensile strength is determined according to the following equation:

$$\sigma_{NT} = \frac{F_{H\max}}{b \cdot h} + \frac{6 \cdot F_{H\max} \cdot y}{b \cdot h^2} \tag{2}$$

Here, F_{Hmax} denotes the maximum horizontal force measured in the load-displacement diagram, b and h the width and the height of the created fracture surface and y the orthogonal distance of the line of impact of the horizontal force to the centre of gravity of the fracture surface area. With numerical curve fitting, the modulus of elasticity may also be determined.

In order to conduct wedge splitting tests at elevated temperatures, a furnace setup with controlled atmospheric conditions is used and combined with *in-situ* optical determination of the opening of the crack mouth during testing [16]. Finally, two measurements per tested temperature were performed for each castable formulation in order to check the reliability of the assessed load-displacement diagrams. Where necessary, a third measurement was performed.

(b) *Thermal shock investigations*

One crucial challenge was to perform efficient thermal cycling at high temperature. To achieve this, a test piece (50 × 50 mm cylinder) is conveyed between two chambers

in a new testing system (Fig. 2). The bottom chamber serves as a standby furnace with the ability to heat or cool the test piece to a predetermined temperature (Fig. 2 (b)). Ascending thermal shocks are achieved in the upper chamber by transporting the test piece into a carbon ring which is inductively heated to incandescence (Chamber 1). The intensive radiation emitted by the carbon ring (susceptor) is particularly efficient to quickly raise the surface temperature of the test piece inside the carbon ring to over 1 800 °C (Fig. 2 (a)). A lifting device ensures the transport of the test piece placed on an alumina tube through the vertically stacked chambers. The system is continuously flushed with inert gas to protect the carbon ring in Chamber 1.

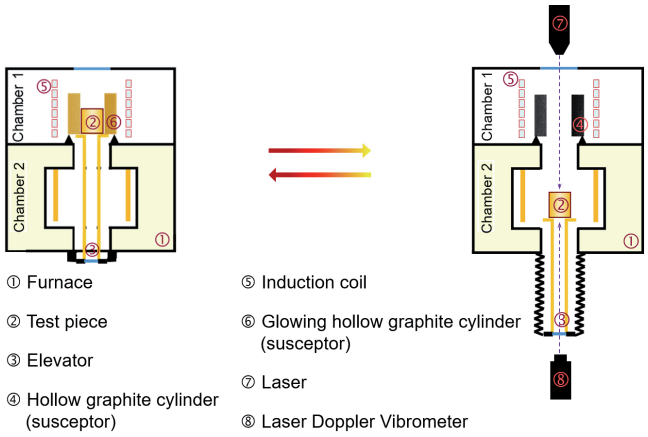

Fig. 2: Schematic representation of the thermal shock testing system and the testing procedure. Preheating and tempering in Chamber 2 **(b, right)**, ascending thermal shock through driving the test piece into an inductively heated carbon ring in the chamber 1 **(a, left)**.

During the thermal cycling, stresses of sufficient magnitude to damage the test piece are generated. The impact of the thermal shocks is assessed quantitatively by measuring the decrease in the ultrasonic velocity inside the test piece, which reflects the deterioration of the mechanical properties of the test piece after having undergone a specified number of thermal cycles. Finally, for a better insight, the thermal damage is quantified using the dimensionless damage parameter D according to Kachanov [17]:

$$D = 1 - \left(\frac{v}{v_0} \right)^2 \qquad (3)$$

where v is the ultrasonic velocity as it propagates through the test piece after thermal cycling and v_0 is the initial ultrasonic velocity as it propagates through the undamaged test piece before thermal cycling. Therefore, D = 0 means no damage, while an increase in the D value signifies increasing damage.

With an emphasis on being relevant for applications in the steelmaking industry, following testing conditions were selected:

– Lower temperature (Chamber 2): 800 °C
– Higher temperature (Chamber 1): 1 600 °C

Five ascending thermal shock cycles were applied to the investigated test pieces as described above. A dwell time of 30 minutes in the bottom chamber (Chamber 2) was selected to ensure the temperature homogeneity of the test pieces. Since thermal stresses tend to quickly reach a maximum during thermal shocking, which roughly corresponds to the maximal temperature difference in the test piece i.e. before its core starts to heat up and the thermal gradient inside of the test pieces gradually flattens out, there is no need to reach temperature homogeneity after applying the thermal shocks. Accordingly, a shorter dwell time (15 minutes) was used in the upper chamber (Chamber 1). The testing conditions were selected to mimic the filling and emptying of a steel ladle, which refractory wear linings experience at temperatures above 1 600 °C when filled with liquid steel and ideally do not drop too low when empty to avoid significant heat loss.

To quantify the resulting damage, the ultrasonic velocity inside the test pieces was measured at room temperature using an experimental laser ultrasonic system applying pulse technique of ultrasonic before and after the thermal cycling [18].

(c) *Thermochemical characterization*

Focusing on the application of the refractories as linings for vessels in the steelmaking industry, the resistance to corrosion of the model refractory castables was evaluated in an induction furnace test. It enables assessment of the corrosion resistance of up eight test pieces simultaneously, under test conditions closed to those experienced by refractories in the steelmaking industry (Fig. 3).

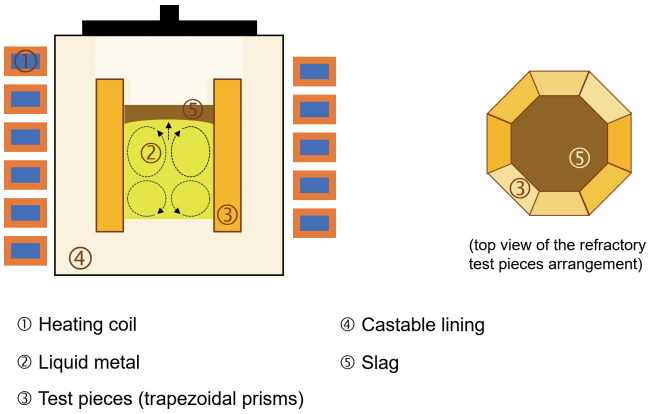

Fig. 3: Schematic representation of the induction furnace test for the investigation of the resistance to corrosion.

The following testing conditions were selected:

– Metal quality: AFNOR XC38/DIN C35 steel,
– Slag composition: CaO/Al_2O_3 = 1,8 with 10 % SiO_2 (simple desulphurization slag),
– Test temperature: 1 650 °C,
– Dwell time at the test temperature: 1 hour.
– The slag was withdrawn once and renewed after 30 min

The metal (~ 16 kg) is heated and melted due to its electrical resistance while exposed to eddy currents generated by alternating electromagnetic fields (f ≈ 9 kHz). Additionally electromagnetic forces and buoyancy ensure a vigorous stirring of the metal melt and the slag respectively.

The eight trapezoid test pieces (segments: 250 mm in length, 57 mm in inner width and 25 mm in thickness) are arranged to form an octagonal crucible in a tiltable

induction furnace. When the metal melt temperature has reached 1 500 °C, 750 g of desulphurization slag is charged. At the end, the metal is completely tapped.

For the assessment of wear, the test pieces (segments) are cut in half lengthwise along their centre lines. Photographs of the cut segments are taken in order to visualize the profile of the corroded zone.

IV. Results and Discussions

(1) Thermomechanical characterization

(a) *Wedge splitting measurements*

When compared to a high-alumina brick (ceramic-bonded), the reference high-alumina colloidal silica-bonded model castable (F-Ref) exhibited much lower mechanical strength (Fig. 4). This is consistent with results from the literature and from the experience of producers and users, especially the low mechanical strength of colloidal-bonded castables is regularly pointed out as one of their most recurrent drawbacks. Above 1 100 °C, it was even not possible to perform relevant measurements, either because the test pieces spontaneously split under the weight of the loading column before reaching the test temperature or no appreciable strength could be measured during the measurement at the intended test temperature. In comparison, measurements could be carried out up to 1 500 °C on the high-alumina bricks. It is assumed that the colloidal silica leads to the formation of a viscous or melt phase in the matrix above 1 000 °C, hence weakening the structural stability of the castable, and in all likelihood promoting creep at relatively low temperature. Even after a dwell time of 1 hour at 1 100 °C, enough silica-rich melt or viscous phase is seemingly (still) present (did not react to form mullite) in order to significantly weaken the material.

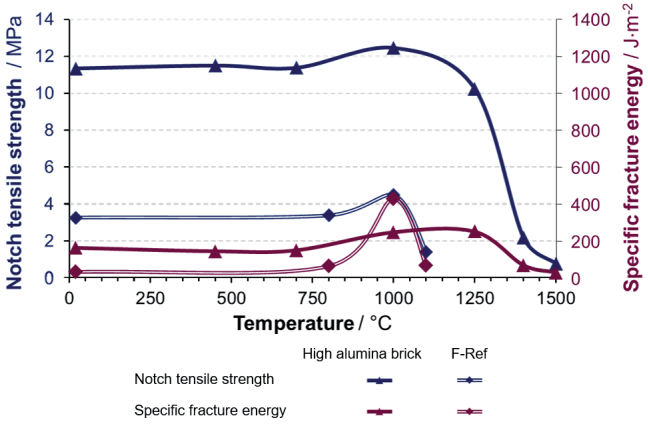

Fig. 4: Evolution of the notch tensile strength and specific fracture energy of the reference colloidal-silica-bonded model castable (F-Ref) and a high-alumina brick with increasing temperature.

Regarding the specific fracture energy, below 1 000 °C only relatively low values were assessed for the reference high-alumina colloidal silica-bonded model castable F-Ref (Fig. 4), mainly because of its low mechanical strength. The high-alumina brick, which displayed, in all likelihood, a similar brittleness in this range of temperature, presented higher specific fracture energy owing to its higher mechanical strength. At 1 000 °C, despite no big change in their mechanical strength, a significant increase of the specific fracture energy of both materials can be observed. The model reference castable F-Ref revealed a value (average of two measurements at the given temperature) that even exceeded that assessed for the high-alumina brick. On the basis of previous measurements on diverse refractory products, this increase indicates the transition from a relatively brittle behaviour to a more ductile behaviour. However, because of the massive weakening of the materials above 1 000 °C and 1 400 °C, respectively, for model reference castable F-Ref and the high-alumina bricks, their specific fracture energy drastically dropped again (cf. Eq. 1). Despite an early drop in its specific fracture energy, the value assessed at 1 000 °C for the model reference castable F-Ref is considerably higher than all values for the specific fracture energy assessed for the high-alumina brick. This strongly suggests that this material could have developed a high level of ductility at high temperature if it had not already been so drastically weakened by 1 100 °C. As the main reason for this weakening is, in all probability, the early formation of a silica-rich melt or viscous phase, while, at the same time, the presence of small amount of melt or viscous phase could be the explanation of the increase of ductility in a first place, there is a strong motivation to limit, and even control, the amount of melt formed in the refractory castable matrix. Hence, a highly ductile material that experiences limited to no weakening up to high temperature could be designed.

Regarding the previous results, only measurements above 1 000 °C were performed for the further investigations to avoid an exceedingly high number of time- and energy-consuming measurements.

In addition and as a complementary approach to evaluate the behaviour of the refractory materials, material properties obtained from wedge splitting measurements can be combined in figure of merits, for instance the brittleness number B, defined as follows:

$$B = \frac{\sigma_t^2 \cdot L}{G_f \cdot E} \tag{4}$$

where σ_t is the tensile strength (that can be substituted with σ_{NT} when comparing results from WST) and L a characteristic dimension of the considered element. The brittleness number B corresponds to the ratio of the elastically stored strain energy at crack initiation to the fracture surface energy necessary to split the element into two pieces. In order to evaluate the brittleness of refractory material without assuming a dimension L, the so-called characteristic length was alternately proposed by Harmuth and Bradt [15], which is inversely proportional to the brittleness number B:

$$L_{Ch} = \frac{G_f \cdot E}{\sigma_t^2} \tag{5}$$

This means that the higher L_{Ch}, the lower the brittleness and accordingly a higher resistance to thermally induced damaging is expected. Actually, L_{Ch} is closely related to the thermal stress damage resistance parameter R'''', where $L_{Ch} = 2 \cdot R''''$ [15].

Regarding the performance of the colloidal-silica-bonded systems, it appears that there is indeed room for improvement as the industrial formulation (IN) demonstrated a more suitable fracture behaviour at 1 000 °C than both reference model castables (Fig. 5 and Table 3). The strength of IN is slightly higher, but above all its specific fracture energy is significantly larger than of F-Ref or C-Ref, leading to higher resistance to material damage. At 1 100 °C, the three materials have a similar ratio specific fracture energy to strength, merely the higher modulus of rupture of the industrial formulation IN promoted a reduction of the brittleness of the material.

The coarsening of the reference model castable formulation (C-Ref) increased significantly its resistance to damage, reflected by a higher L_{Ch} compared to F-Ref (Fig. 5 and Table 3). This is mainly driven by the increase of the ratio of specific fracture energy to strength. Coarsening the refractory castable led to a slightly weaker material, but with an increased capability to resist to crack propagation.

Table 3: Measured thermomechanical properties for the reference high-alumina colloidal-silica-bonded model castables (F-Ref and C-Ref) the commercially available castable (IN) and the colloidal-spinel-bonded model castables (CSPS30 and CSPS50). Two measurements per temperature.

Castable	Temperature/°C	G_f'[1)]/J·m^{-2}	σ_{NT}/MPa	E[2)]/MPa	L_{Ch}/mm
F-Ref	1 000	425	4,5	13,7	290
	1 100	65	1,4	6,8	235
C-Ref	1 000	397	3,7	11,5	331
	1 100	98	1,5	7,0	290
IN	1 000	778	5,3	11,0	307
	1 100	54	1,2	8,0	323
CSPS30	1 000	39	1,0	3,4	141
	1 100	45	0,6	3,0	330
	1 250	248	1,3	2,5	393
	1 500	151	0,8	1,2	275
CSPS50	1 000	56	1,3	7,5	266
	1 250	458	1,7	3,3	493
	1 500	199	1,0	1,8	375

1) G_f': specific fracture energy calculated up to a drop of 90 % in the maximum load
2) Indicative value assessed from the load-displacement diagrams

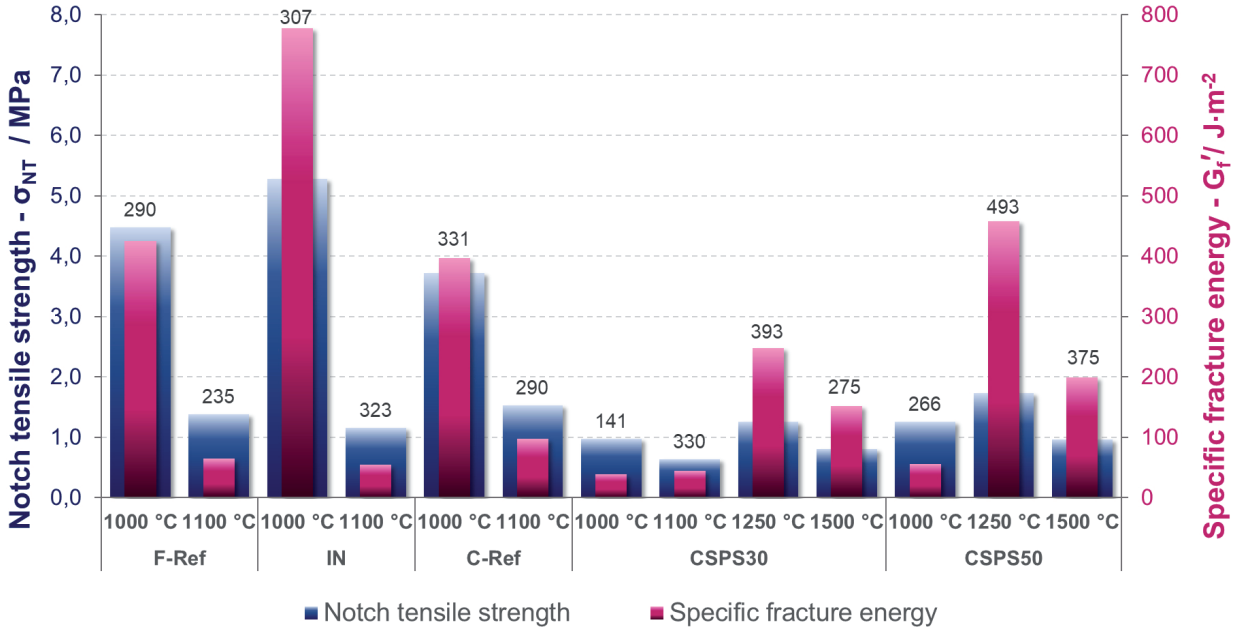

Fig. 5: Assessed values of notch tensile strength and specific fracture energy for the reference high-alumina colloidal-silica-bonded model castables (F-Ref and C-Ref), the commercially available castable (IN) and the colloidal-spinel-bonded model castables (CSPS30 and CSPS50). The number above each column corresponds to the characteristic length L_{Ch} for the given castable.

At a first glance, the colloidal-spinel-bonded model castables (CSPS30 and CSPS50) seemed to be weaker than their colloidal-silica-bonded counterpart (C-Ref), exhibiting a lower value of mechanical strength and specific fracture energy below 1 100 °C. However, while the reference colloidal-silica-bonded model refractory test pieces (F-Ref and C-Ref) became too weak to be tested above 1 100 °C, failing already during heating under the weight of the loading column or presenting no appreciable strength at the intended test temperature, measurements on colloidal-spinel-bonded model castable test pieces (CSPS30 and CSPS50) could be performed up to 1 500 °C (Fig. 5 and Table 3). Their mechanical and fracture behaviour was even improved at 1 250 °C and still remained better than below 1 100 °C at a test temperature of 1 500 °C. The comparatively weak performance of the colloidal-spinel-bonded model castables below 1 100 °C is probably linked to the poor green strength of the materials. Only once the materials start to sinter and new phases formed (above 1 100 °C), in all likelihood without the formation of a significant quantity of viscous or liquid phase, the colloidal-spinel-bonded model castables develop outstanding mechanical and fracture properties. Accordingly, by improving the green strength of the colloidal-spinel-bonded model castables, generally enhanced behaviour, over a larger range of temperatures, can be expected. A first attempt, to improve the green strength of the colloidal-spinel-bonded model castable was made by increasing the content of solid colloidal in the sol (CSPS50). This indeed results in an improvement of the mechanical and fracture behaviour at the investigated temperatures, as the test pieces made of CSPS50 outperformed test pieces of CSPS30 (higher mechanical strength, specific fracture energy and characteristic length). Finally, reducing the particles sizes in the colloidal spinel suspensions, to sizes similar to those of the commercial silica sol (Table 2), should further improve the mechanical and fracture properties of the colloidal-spinel-bonded castables, in particular by improving their sintering behaviour at higher temperatures.

(b) ***Thermal shock investigations***

Before characterization of the different developed refractory model castable formulations, a rudimentary assessment of the repeatability of the thermal shock resistance measurements performed with the high-temperature testing device was carried out. To this end, two measurements were carried out on two test pieces (50 × 50 mm, F-Ref-1 and F-Ref-1') cut from the same item (50 × 102 mm) and one test piece (F-Ref-2) from another item, both items were made of the reference high-alumina colloidal-silica-bonded model castable formulation. Even before thermal shocks were performed, slight differences in ultrasonic velocity were noticed among the test pieces (Fig. 6 and Table 4). These indicate some variation in density and/or the presence of diverse random microstructural defects, such as pores and microcracks, independent of whether the test pieces were cut from the same item or different items. To some extent, this is related to the intrinsic heterogeneous nature of refractory materials as coarse ceramics. After thermal cycling, damage levels D ranging from 0,29 to 0,36 were assessed (Table 4). With the necessary cautiousness regarding the very limited number of test pieces involved, it did not matter whether the test pieces were cut from the same item or different items. But all in all, differences in the level of damage D ranging from 0,27 to 0,38 cannot be regarded as significant for the model castables and should be considered as a good performance based on previous experiences.

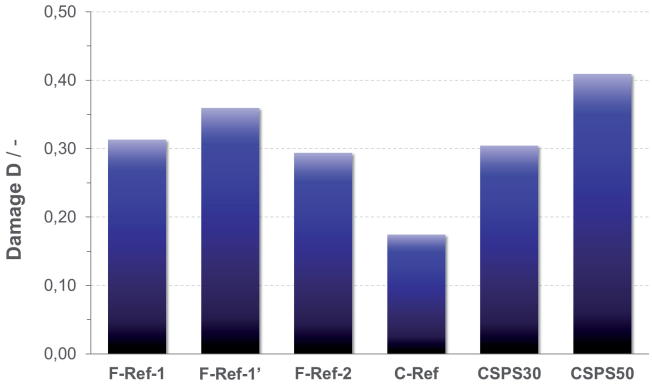

Fig. 6: Level of damage D assessed using the laser-ultrasonic system after five thermal cycles for all investigated high-alumina colloidal-bonded model castables.

Table 4: Results of the resistance to thermal shock investigations (five thermal cycles between 800 °C and 1 600 °C). The ultrasonic velocity values are the average of three measurements.

Castable	Ultrasonic/m·s^{-1}		Damage D/-
	before thermal cycling	after thermal cycling	
F-Ref-1	5 046	4182	0,31
F-Ref-1′	4 841	3874	0,36
F-Ref-2	4 872	4095	0,29
C-Ref	3 317	3014	0,17
CSPS30	2 730	2276	0,30
CSPS50	2 803	2154	0,41

Consistent with the wedge splitting measurements, the coarsening of the reference model castable formulation (C-Ref) significantly increased its resistance to thermal shocks. In fact, of all the formulations investigated, this formulation (C-Ref) demonstrated the best resistance to thermal shocks under the applied testing conditions, with a damage parameter value D of only 0,17 after the high-temperature thermal shocks. Furthermore, the lower assessed value of ultrasonic velocity before thermal cycling confirmed the lower density and/or higher share of defects in C-Ref in comparison with F-Ref. A higher of share of defects initially present in the material is expected, to a certain extent, to improve the resistance to thermal shocks.

The colloidal-spinel-bonded model castable with the lower solid content in the sol (CSPS30) performed as well as the reference colloidal-silica-bonded model refractory castable F-Ref. Accordingly, CSPS30 displayed a higher level of damage D than reference model refractory castable C-Ref, which could be linked with its even lower assessed value of ultrasonic velocity before thermal cycling (actually the lowest assessed in the present investigations), potentially reflecting a poorly bonded material after casting and curing. However, the colloidal-spinel-bonded model castable with the higher solid content in the sol (CSPS50) and slightly better bond according to the ultrasonic velocity and the wedge splitting measurements (Fig. 5 and Table 3) did not perform better. This suggests that other mechanisms are involved. It is assumed that the formation of a viscous phase or a melt at high temperature, despite impairing the mechanical and fracture resistance of the material, helped to improve the resistance to thermal shock of the reference colloidal-silica-bonded model refractory castables (F-Ref and C-Ref). The assumed presence of a viscous or liquid phase, at approx. 1 100 °C, should promote stress relief in the thermally shocked material. The colloidal-spinel-bonded model refractory castables, free of amorphous silica, are expected to form a smaller quantity of viscous/liquid phase at much higher temperature than colloidal-silica-bonded model refractory castables. The addition of a small quantity of colloidal silica to the colloidal spinel suspension may help to increase the green strength of the resulting colloidal-bonded model refractory castable as well as improve its resistance to thermal shock while having a minimal impact on their structural stability at high temperature.

(2) Thermochemical characterization

After completion of the induction furnace test and cutting of the test pieces (segments) in half, photographs of the corroded cut segments were taken and processed using the image manipulation program GIMP in order to evaluate more precisely the extent of the corrosion. For practical classification purposes, the area of the segments that were completely worn away during the corrosion test are called the corroded area, while the area of the segments where the slag has penetrated the test pieces without leading to their breakup at the end of the test are referred to as the infiltrated area (Fig. 7).

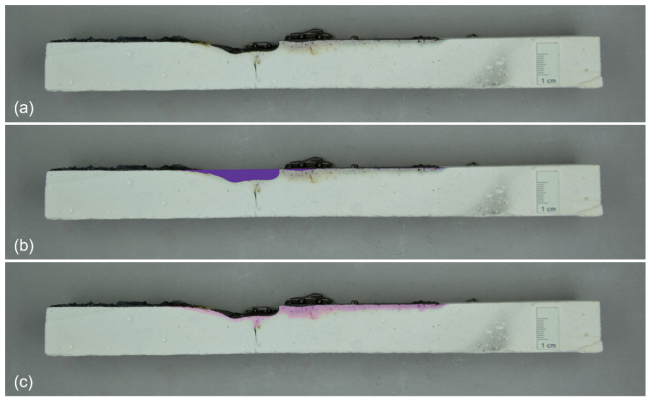

Fig. 7: Example of a photograph of a corroded cut segment (a) raw picture, (b) corroded area in violet and (c) infiltrated area highlighted in translucent fuchsia.

During one induction furnace test, up to eight different segments can be simultaneously tested. However, to ensure the reliability of the results, only four different colloidal-silica-bonded formulations and accordingly two segments of each colloidal-silica-bonded refractory castable were investigated during a single induction furnace test. This means that four half-segments were available per refractory castable formulation for a basic statistical evaluation.

The coarsening of the reference formulation (C-Ref), as well as the addition of spinel aggregates AR 78, seems to slightly improve the resistance to corrosion of the high-alumina colloidal-silica-bonded model castable. Both the assessed corroded and infiltrated areas were lower than for F-Ref, but still within its standard deviation (Table 5 and Fig. 8). Coarsening a refractory product microstructure reduces the share of the fine matrix that is preferentially attacked by the corrosive medium because of its high specific area, and hence coarsening tends to enhance the resistance to corrosion. Spinel is also known to promote higher resistance to corrosion.

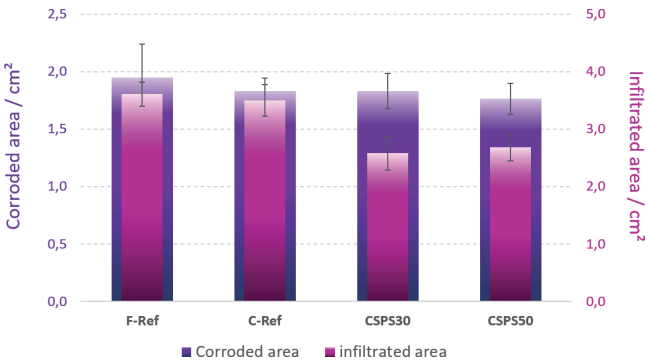

Fig. 8: Assessed values for the corroded and infiltrated areas (including standard deviation) of the investigated high-alumina colloidal-bonded model castables.

While the use of colloidal spinel, instead of colloidal silica, as a bonding system significantly limited the infiltration by the corrosive medium (i.e. reduced the assessed infiltrated area), it seems to have a much more moderate impact on the corroded area. The colloidal-spinel-bonded model castable with the lower solid content in the sol

Table 5: Results of the resistance to corrosion for the investigated colloidal-bonded model castables (four half segments per castable).

Castable	Corroded area (cross-section)/cm²		Infiltrated area (cross-section)/cm²	
	mean	standard deviation	mean	standard deviation
F-Ref	1,95	0,29	3,60	0,21
C-Ref	1,83	0,11	3,49	0,28
CSPS30	1,82	0,16	2,58	0,29
CSPS50	1,76	0,14	2,68	0,23

(CSPS30) displayed the same amount of corroded area as the reference colloidal-silica-bonded model refractory castable C-Ref. However, increasing the solid content in the sol (CSPS50) led to a slight reduction of the corroded area. Spinel is expected to be less prone to react with most corrosive media than alumina and already used in high-end industrial high-alumina refractory castables to improve their resistance against corrosion. The assessed effect in the present study remained moderate, but nonetheless significant to mitigate the infiltration by the corrosive medium. Furthermore, while not directly investigated in the present study, colloidal spinel as bonding system is anticipated to display enhanced stability when exposed to reducing conditions [19], which are expected to gain in prominence as processes using hydrogen are on the rise [20].

V. Conclusions

While a refractory castable without reasonable placing properties may have some difficulties in gaining acceptance for applications in the industry, a refractory product with a poor high temperature behaviour will simply find no use at all. In both cases, the bonding phases of refractory castables play a central role. In the present study, the high-temperature performance of colloidal-silica-bonded and colloidal-spinel-bonded model refractory castables were investigated.

The mechanical and fracture behaviour of the developed model high-alumina colloidal-bonded refractory castables was assessed with wedge splitting measurements. The resistance to thermal shock was investigated using a new testing system that enables ascending (fast irradiation heating) thermal shocks repeatedly applied to refractory test pieces previously heated at a defined temperature. Hence controlled temperature changes triggered at the surface of test pieces were performed, thus enabling a tailored investigation of the thermal shock resistance of model colloidal-bonded refractory castables for application in the steelmaking industry. Finally, induction furnace tests were performed to investigate the resistance to corrosion of the colloidal-bonded refractory castables in conditions mimicking application in the steelmaking industry.

The investigated colloidal-silica-bonded high-alumina model refractory castables displayed relatively modest strength and wedge splitting measurements could not be performed at temperature above 1 100 °C. The formation of viscous or liquid phases from colloidal silica was assumed to jeopardize the structural stability of the refractory castable above 1 100 °C. However, the colloidal-silica-bonded castables seem to develop a rather ductile behaviour quite early (1 000 °C) and exhibited a high resistance to thermal shocks.

The use of colloidal spinel instead of colloidal silica as a bonding system resulted in weak mechanical properties after casting, which was reflected in low values for mechanical strength and specific fracture energy at moderate temperature. However, unlike for colloidal-silica-bonded model refractory castables, wedge splitting measurements on the colloidal-spinel-bonded model castable test pieces could be performed up to 1 500 °C. Their mechanical and fracture behaviour was even improved at 1 250 °C and still remained better than below 1 100 °C at a test temperature of 1 500 °C. Concurrently and depending on the share of spinel in the colloidal suspension, the colloidal-spinel-bonded model castables displayed good resistance to thermal shocks, quite similar to their reference colloidal-silica-bonded model refractory castables equivalent. This could potentially be improved by promoting the formation of a very small amount of viscous or liquid phase, which should not impact drastically the mechanical properties at high temperature while enabling the relief of thermal stresses. Finally, a slight improvement of the corrosion resistance of colloidal-spinel-bonded model castables compared to the reference colloidal-silica-bonded model refractory castables could be determined. All in all, the developed colloidal-spinel-bonded castables already displayed decent high-temperature behaviour, but most importantly colloidal-spinel-bonded high-alumina castables have considerable potential for application in extreme environments (very high refractoriness, relative inertness to reducing atmosphere) and, as a relatively new bonding system, large scope for improvement.

Acknowledgements

We would like to thank the German Federation of Industrial Research Associations (AiF) and the Public Service of Wallonia (SPW), Belgium for the financial support of the research project "ColCast" (IGF-No. 305 EN, Germany, and agreement no. 2010279, Belgium). This project was implemented under the CORNET initiative and carried out under the auspices of AiF and financed in Germany within the budget of the Federal Ministry for Economic Affairs and Climate Action (BMWK) through the programme to promote collective industrial research (IGF).

References

1 Ismael, M., Anjos, R.D., Salomão, R., Pandolfelli, V.C.: Colloidal silica as a nanostructured binder for refractory castables, *Refract. Appl. New.*, **11**, 16, (2006).

2 Xiong, J.Q., Peng, Y.T., Da, Y.X., Mao X.S.: The characteristics of silica-sol combining refractories, *Adv. Mat. Res.*, 396 – 398, (2011).

3 Souri, A., Kashani, N.F., Sarpoolaky, H.: Improving thermo-mechanical properties of tabular alumina castables via using nano structured colloidal silica. In: Proceedings of 1st International Conference on Nanomaterials: Applications and Properties. Crimea, Ukraine, 2011.

4 Braulio, A.L., Tontrup, C., Medeiros, J., Pandolfelli, V.C.: Colloidal alumina as a refractory binder, In: Proceedings of the 35th Alafar Congress, Lima, Peru, 2010.

5 Singh, A.K., Sarkar, R.: Synthesis and characterization of alumina sol and its use as binder in no cement high-alumina refractory castables, *Int. J. Appl. Ceram. Technol.*, **12**, S3, 54 – 60, (2015).

6 Nouri-Khezrabad, M., Braulio, M.A.L., Pandolfelli, V.C., Golestani-Fard, F., Rezaie, H.R.: Nano-bonded refractory castables, *Ceram. Int.*, **39**, [4], 3479 – 3497, (2013).

7 Giovannelli Maizoa, I.D., Luz, A.P., Pagliosa, C., Pandolfelli, V.C.: Boron sources as sintering additives for alumina-based refractory castables, *Ceram. Int.*, **43**, 10207 – 10216, (2017).

8 Luz, A.P., Lopes, S.J.S., Gomes, D.T., Pandolfelli, V.: High-alumina refractory castables bonded with novel alumina-silica-based powdered binders, *Ceram. Int.*, **44**, 9159 – 9167, (2018).

9 Wang, F., Chen, P., Li, X., Zhu, B.: Effect of micro-spinel powders addition on the micro-structure and properties of alumina refractory castables, *Ceram. Int*., **45**, 2989 – 2999, (2019).

10 Mukhopadhyay, S., Pal, P., Nag, B., Jana, P.: Influence of gel-derived nanocrystalline spinel in a high alumina castable: part 2, *Ceram. Int.*, **33**, 175 – 186, (2007).

11 Singh, A.K., Sarkar, R.: Development of spinel sol bonded high pure alumina castable composition, *Ceram. Int.*, **42**, [15], 17410 – 17419, (2016).

12 Singh, A.K., Sarkar, R.: Urea based sols as binder for nano-oxide bonded high alumina refractory castables, *J. Alloy. Compd.*, **758**, 140 – 147, (2018)

13 Ghosh, S., Maiti, T., Sen, S, Mukhopadhyay, S.: Influence of gel-derived nanocrystalline spinel in a high alumina castable: part 1, *Ceram. Int.*, **31**, 333 – 347, (2005).

14 Abdelouhab, S., Petit, A., Delmotte, C., Brochen, E., Dannert, C., Krause, O.: Advancements in refractory castables: Enhancement of green-state and high-temperature properties of colloidal spinel bonded castables, In: Proceedings of the 66th International Colloquium on Refractories (ICR), Aachen, Germany, 2024.

15 Harmuth, H., Tschegg, E.K.: A fracture mechanics approach for the development of refractory materials with reduced brittleness, *Fatigue Fract. Eng. Mater. Struct.*, **11**, [20], 1585 – 1603, (1997).

16 Brochen, E., Dannert, C., Quirmbach, P.: Thermo-Mechanical Characterisation of Magnesia-Carbon Refractories by Means of Wedge Splitting Test under Controlled Atmosphere at High-Temperature, In: Proceedings of the 13th Unified International Technical Conference on Refractories (UNITECR), Victoria, Canada, 2013.

17 Kachanov L.M.: Introduction to Continuum Damage Mechanics. Mechanics of Elastic Stability. Dordrecht, Boston, Lancaster: Martinus Nijhoff Publishers, 1986.

18 Brochen, E., Dannert, C., Klose, J., Esch, S., Kohns, P., Ankerhold, G. Application of the laser ultrasonic technology to the characterisation of refractory materials, In: Proceedings of the 65th International Colloquium on Refractories (ICR), Aachen, Germany, 2022.

19 Gomes, M.R., Leber, T., Tillmann, T., Kenn, D., Gavagnin, D., Tonnesen, T., Gonzalez-Julian, J.: Towards H_2 implementation in the iron- and steelmaking industry: state of the art, requirements, and challenges for refractory materials, *J. Eur. Ceram. Soc.*, **44**, 1307 – 1334, (2024).

20 Somers, J.: Technologies to decarbonise the EU steel industry, European Commission, Joint Research Center, Luxembourg, 2022, doi: https://doi.org/10.2760/069150.